Journal of Magnetism and Magnetic Materials 475 (2019) 421–428

Contents lists available at ScienceDirect

Journal of Magnetism and Magnetic Materials

journal homepage: www.elsevier.com/locate/jmmm

Research articles

Probing particle-matrix interactions during magnetic particle spectroscopy

James Wells*, Norbert Löwa, Hendrik Paysen, Uwe Steinhoff, Frank Wiekhorst

Physikalisch-Technische Bundesanstalt, Abbestraße 2-12, 10587 Berlin, Germany

A B S T R A C T

Interactions between magnetic nanoparticles (MNPs) and their surrounding matrix were investigated during temperature-controlled magnetic particle spectroscopy (MPS). MNPs are used as tracers in emerging biomedical imaging technologies, including magnetic particle imaging (MPI), which employ spatially inhomogeneous time-varying magnetic fields to generate imaging signals. For safe and reliable imaging procedures, it is important to understand the thermal and mechanical interactions between MNPs and the surrounding biological matrix. We performed in-vitro investigations using magnetic field hyperthermia (MFH) and temperature-controlled MPS to elucidate the excitation-field dependent MNP-matrix interaction. MFH measurements of ferucarbotran (FCT) MNPs were conducted using a low-frequency, high-amplitude, set-up designed to emulate the typical field conditions employed in MPI. First, it was tested whether concentrated FCT samples produce measurable heating in MFH characterization. A strong bulk heating effect ($\Delta T = 40$ K) was observed, showing that the individual MNPs dissipate a significant quantity of heat. However, no measurable bulk temperature increase occurred during MFH of dilute FCT preparations in liquid or gelatin suspensions. Then, temperature-controlled MPS measurements were performed on dilute FCT immobilized in gelatin. The melting transition of the dilute gelatin preparation produced a clear change in the temperature-dependent MPS spectra. The melting transition was reproducible between measurements using the same field excitation, with a standard deviation of $\sigma = 0.2$ K. The melting transition temperature was found to depend upon the amplitude of the MPS excitation field. A reduction in the melting transition onset temperature of 2.3 K was observed when the excitation amplitude was increased from 6 mT to 25 mT. This shift is attributed to increasing mechanical and thermal particle-matrix interactions at higher excitation fields. The results show that within the studied system, individual MNPs interact with their local environment in a non-negligible way during MPS measurement, even when bulk heating of the sample is not detected. Our findings hold significance for the potential impact of MPI and related technologies on living tissues, a subject deserving of further study.

1. Introduction

Magnetic particle imaging (MPI) is a novel medical imaging modality which maps the spatial distribution of a magnetic nanoparticle (MNP) tracer [1] via dynamic magnetization measurements. The technique uses a sinusoidal drive-field excitation (common frequencies between 1 kHz and 150 kHz, amplitudes between 5 and 90 mT peak) to probe the medium being imaged. The measured magnetization response of superparamagnetic magnetic nanoparticles (MNPs) contains additional higher harmonics of the drive-field frequency, due to the non-linear and frequency-dependent magnetization characteristics of MNPs. These higher harmonics provide a unique fingerprint of the nanoparticles contained within the sample, which is used as the basis for image reconstruction in MPI [2]. A steep DC gradient field which passes through zero at a single location (field free point (FFP)) is used to saturate the nanoparticles across the majority of the MPI imaging volume, so that imaging signal is only produced from a small volume surrounding the FFP. By scanning the FFP throughout the imaging volume, the MPI signal produced at each location can be measured, allowing images to be reconstructed [3].

The imaging signal produced in MPI is dependent upon the frequency and amplitude of the excitation fields used, the type of MNP used as a tracer, the MNP quantity present, and local environment factors including the MNP binding state and temperature. MPI image reconstruction techniques typically map the nanoparticle concentration measured within each image voxel, with iron sensitivities in the low nanogram range [4,5]. More recently, so-called “multi-color” reconstruction techniques have been used to map additional parameters such as MNP type, binding state, or temperature [6–8].

Magnetic particle spectroscopy (MPS) is a technique closely related to MPI. MPS measurements are conducted using a magnetic particle spectrometer. In essence, this is an MPI scanner with no spatial encoding (no additional field gradient). MPS is most commonly used as a fast and highly sensitive method for the characterization of MNP samples, to test their suitability as MPI tracers. The sensitivity of MPS spectra to local MNP viscosity or immobilization has been previously noted using temperature-dependent MPS measurements of MNPs distributed in gelatin [9]. The dynamics of nickel nanorods in gelatin under alternating magnetic fields was also previously investigated by monitoring the transmission of a linearly polarized laser light [10].

MPI and MPS technologies are commonly described within the literature as being minimally- or non-invasive. This is due to the lack of

* Corresponding author.
E-mail address: james.wells@ptb.de (J. Wells).

https://doi.org/10.1016/j.jmmm.2018.11.109
Received 20 June 2018; Received in revised form 21 November 2018; Accepted 22 November 2018
Available online 23 November 2018

ionizing radiation or intrusive surgical probes, the biocompatibility of iron-oxide nanoparticles [11], and the selection of drive-field characteristics to minimize tracer heating or nerve stimulation during excitation. MPI/MPS studies typically use MNPs and excitation fields which are selected to minimize or prevent the dissipation of macroscopically measurable quantities of heat. MPI has been successfully demonstrated for in-vivo studies within animal models [12–14], although a detailed study of the health implications is still required.

One of the applications for which MPI and MPS have attracted interest is the in-vivo tracking of cells labelled with MNP. In [14] and [15], ferucarbotran (FCT) labelled human mesenchymal stem cells were successfully tracked in-vivo after transfection using MPI at a drive frequency of 20 kHz. These highly valuable works clearly demonstrated the sensitivity of MPI for locating MNP labelled cells after migration to different parts of a rodent physiology, although they offer little insight into the strains experienced by the loaded cells during MPI measurements, or the long-term impact of the measurement procedures. Nanoparticles internalized into red blood cells have also been proposed as a possible method for prolonging the half-life of MPI tracers for in-vivo MPI [16], although the specific impact of the MPS measurements on the MNP loaded cells is not reported.

The effect of MPS excitation fields on living cells after uptake of very small iron oxide nanoparticles with average hydrodynamic diameter of 8 nm was briefly investigated in [17]. No negative impact was found on cell viability or proliferation during seven days after MPS exposure. These MNPs were used in this study as their exceptionally small size facilitated easy cell-internalization, although they offer insufficient MPI signal for good image reconstruction, either before or after internalization. The properties which typically allow MNPs to produce strong MPI signals have been previously investigated, with optimal results reported for particles which have larger overall magnetic moments and sizes [18]. Larger MNPs, particularly those with a multicore structure, are also linked to greater potential to dissipate heat [19,20]. In addition to this, larger magnetic moments will exert greater mechanical strain on the local surroundings. So far, no detailed study has yet been undertaken to investigate the specific impact of common MPI tracer probes on their local surroundings during MPI or MPS field excitation, or the potential impact on biological tissues which could result.

Magnetic field hyperthermia (MFH) describes the underlying mechanism of an emerging cancer treatment [21] based on the distribution of MNPs within tumor tissue, and the subsequent infliction of damage to the cancer cells via heat generated by applying high frequency (typically 250–900 kHz) AC magnetic fields. The technique has enjoyed significant interest in recent years, and is currently undergoing evaluation in clinical trials [22,23] as well as a range of in-vitro and in-vivo studies. At present, characterization of MNPs as MFH agents is generally done by exciting a sample of MNPs and measuring the resultant bulk increase in the temperature of the MNP suspension sample. However, recent studies have indicated that cell damage can occur during MFH, even when the macroscopic heating of the sample generated by the MNPs is negligible, or well below the threshold for thermoablation [24,25]. Additional measurements have suggested two potential mechanisms for these observations. These are the generation of localized microscopic hot-spots at the site of each nanoparticle exposing the immediate surroundings to greater temperatures than the macroscopic fluid [24], or the effects of mechanical stress and abrasion on cells [26]. Additional studies have recently demonstrated the potential of steep field gradients to exert sufficient forces on intracellular MNPs to disrupt the function and bio-structures of cancer cells [27]. The discovery that MNPs under AC magnetic fields can cause cell damage without generating measurable macroscopic heating is of great importance for MPI development. It suggests that a microscopic understanding of the interaction between MNPs and the surrounding matrix during MPI or MPS is required, rather than the measurement of macroscopic heating of bulk samples of MNP suspension. The interaction of MNPs with their immediate surroundings during MPI measurement must be understood before the technology can be truly validated as safe for clinical use.

In this work we present preliminary in-vitro studies which we use to investigate the following hypothesis: MNP probes interact with their local environment in a non-negligible way during MPI or MPS. This interaction is a result of mechanical strain and/or heating (whether local to individual nanoparticles or a bulk effect). This interaction will be dependent on the amplitude and frequency of the excitation field used, and should be clearly understood for the design and implementation of safe in-vivo MPI.

2. Theory of particle-matrix interactions during MPI and MPS

Different possibilities exist for how MNPs undergoing AC field excitation may interact with their surrounding matrix. The precise contributions in each case will depend upon the characteristics of the MNPs used, and the excitation field applied. Two primary mechanisms may exert mechanical strain on the immediate surroundings of individual nanoparticles. First, reversals in the direction of the AC excitation field may produce a varying torque as the nanoparticles attempt to rotate via Brownian processes and align their moments (see Fig. 1(a)). Many of the leading MNP candidates for MPI tracers are multicore or “nanoflower” particles containing large numbers of very small MNPs closely aggregated in disordered arrangements (although some single-core MNP tracers have also been investigated [28,29]). The anisotropy of multicore MNPs is complex [30]. However, assuming that a MNP exhibits some degree of overall anisotropy, and that the MNP’s moment is not aligned with the field, a torque (τ) will be exerted

$$\tau = m \times B$$

where m is the particle moment and B the magnetic flux density.

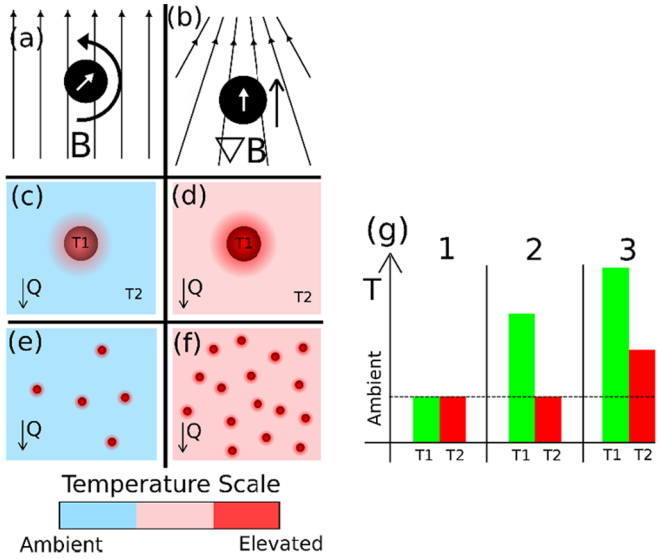

Fig. 1. Illustrations of particle-matrix interactions possible during AC field excitation. (a) torque (black curved arrow) exerted as particle moment (white arrow) orientates with the homogeneous field (B), (b) translational movement (black arrow) due to field inhomogeneity (∇B). (c) Heat generated by magnetic excitation may result in just heating confined to the location of the particle (T1 = particle temperature). A broader heating of the bulk suspension fluid (T2 = macroscopic fluid temperature) may also result (d). The T2 value achieved during measurement is concentration dependent (e–f). The arrow labelled Q in (c-f) represents heat loss from the MNP suspension into the wider environment. Three combinations for local MNP temperature and bulk fluid temperature are shown in (g) (green: T1, red: T2; 1: equilibrium before magnetic excitation, 2: MNPs heated, heat deposition in the matrix is insufficient to create a significant temperature rise in the matrix, 3: MNPs heated, heat dissipation in the matrix causes significant temperature rise in the matrix).

A second source of mechanical strain can also arise. If the magnetic excitation field is strongly inhomogeneous, then MNPs will undergo translational forces due to the field gradients which they experience (Fig. 1(b)). The translational force exerted under these conditions is given by

$$F = (m \bullet \nabla)B$$

If F or τ are of sufficient amplitude, the drag forces exerted by the suspension medium may be overcome, and substantial particle movement can occur. In the case of MNPs suspended in water or another fluid, the drag forces will be dictated by the viscosity of the fluid, and the particle's hydrodynamic diameter. Binding events between the MNP surface and biomolecules contained within the dispersion medium can influence the drag forces considerably. Significant amplitudes of AC field excitation, as well as steep field gradients, are key to the operation of MPI scanners [3]. This means that each of these mechanical strain components can be expected to occur during measurements using a spatially encoded MPI scanner. For MPS measurements, translational forces will be reduced as there is no gradient field, but rotational torque will still be induced.

In addition to mechanical strain on the surrounding matrix, MNPs will dissipate magnetic energy into heat as they undergo Brownian and/or Néel processes induced by the excitation field. Measurements of macroscopic temperature rise in MNP suspensions during AC field excitation are well established. Based on these macroscopic measurements, the specific absorption rate (SAR) is a common parameter used in the literature to characterize the bulk heating efficiency of specific nanoparticle preparations [31]. The possibility for local hotspots to exist in the immediate vicinity of individual nanoparticles will be heavily dependent on the thermal coupling between specific nanoparticle types and the surrounding matrix, the extent of the heat generated (determined by the nanoparticle composition and the field frequency and amplitude), and the location of heat generation (at the particle surface, or interior), and the rates of heat diffusion within each material.

Fig. 1(c) illustrates a case in which the excitation field elevates the local temperature of a MNP. However, the rate at which heat dissipates into the surrounding fluid, and the rate at which heat escapes from the MNP suspension into the environment (Q), mean that the surrounding fluid is not measurably heated above the ambient temperature. Fig. 1(d) illustrates the case in which the heat dissipated by the particles is sufficient to overcome the rate of heat escape from the system, with a resultant elevation of the bulk fluid temperature. Note that the local temperature of the nanoparticle (T_1) is still elevated above the wider temperature (T_2) of the fluid in both Fig. 1(c) and (d). Fig. 1(e) and (f) illustrate how differing concentration can influence T_1 and T_2 for a given MNP type and field excitation. In both 1(e) and 1(f), the individual MNPs are generating the same amount of heat, resulting in elevated local temperatures. In (e) the low concentration of particles means that there is no increase in T_2, while the higher concentration in (f) results in a measurable T_2 increase. Possible cases for T_1 and T_2 during MPI are shown in Fig. 1(g). In case 1, neither the MNPs nor the carrier fluid experience increased temperatures. In case 2, the MNPs are heated, but the bulk fluid remains at ambient temperature. In case 3, both the MNPs and the carrier matrix show an elevated temperature, with the temperature of the MNPs higher than that of the surrounding fluid.

In the following, we describe a set of complimentary experiments designed to probe the interaction between MNPs and their surrounding matrix during excitation at MPI frequencies.

3. Materials and methods

3.1. Magnetic nanoparticle preparations

Experiments were conducted using the common MPI tracer Ferucarbotran (FCT) (Meito Sangyo, Japan). Each FCT MNP consists of a large number of very small iron oxide cores embedded in a dextran matrix, with an average hydrodynamic size for the FCT particles of 60 nm [32]. It should be noted that FCT contains a distribution of particle sizes and magnetic moments, as was reported in [18]. The material forms the basis of the FDA approved MRI contrast agent Resovist, used for liver imaging. FCT has been used extensively as a tracer in MPI research [33], due to its good imaging qualities and existing approval for use in humans.

Table 1
FCT sample types and respective iron concentrations used in the reported experimental studies.

Sample	Matrix	Iron Concentration (mmol/L)
FCT-Liquid (c(Fe) High)	Aqueous	935
FCT-Liquid (c(Fe) Low)	Aqueous	7
FCT-Freeze Dried	Mannitol	~ 2
FCT-Gelatin	Gelatin 1%	5

FCT was implemented in a variety of different preparations (see Table 1). Two liquid preparations (FCT-LIQ), one with a high iron concentration c(Fe) = 935 mmol/L and one with a low concentration c(Fe) = 7 mmol/L. Dilute FCT nanoparticles were immobilized in a 1% gelatin matrix (FCT-GEL) with an iron concentration of c(Fe) = 5 mmol/L. In addition, FCT nanoparticles were freeze dried in a mannitol matrix as an example of a strongly immobilized system. Iron concentration of FCT samples were measured by spectrophotometry using a phenanthroline assay.

Key considerations for maximizing the reproducibility of samples during repeated measurements include minimizing the time that the sample spent at elevated temperatures (to reduce the possibility of gelatin molecules being denatured), redistribution of the sample via vortexing after each measurement run before sample resolidification, and following the same resolidification procedure (temperature, time etc.). These laborious sample-control techniques may be avoided by using a fresh FCT-GEL sample (from the same production batch) for each measurement curve. This was the method employed in the measurements reported here.

3.2. Low-frequency magnetic field hyperthermia (LF-MFH) efficiency measurements

The heating efficiency of magnetic nanoparticle dispersions undergoing excitation fields in the MPI relevant range was measured using a custom-built non-adiabatic apparatus [34]. The device operates at a lower frequency (79 kHz) than is typically used when evaluating nanoparticles for therapeutic applications (250–900 kHz), and provides variable field amplitudes up to around 10 mT. Therapeutic hyperthermia characterization measurements tend to focus on comparatively low amplitudes and high frequencies. However, MPI scanners typically implement somewhat lower frequencies (to minimize heating) and higher amplitudes, making the LF-MFH system a useful tool for probing heat generation and particle-matrix interactions under the sort of conditions more commonly encountered in MPI or MPS.

The LF-MFH apparatus uses a sample volume of 400 μL contained within an Eppendorf tube. The sample is placed at the center of the excitation coil. Water-cooling of the excitation coil and polystyrene insulation layers were used to decouple the joule heating of the coil from the MNP hyperthermia occurring within the sample under evaluation. Thermal insulation also minimized heat loss from the ferrofluid sample undergoing measurement. A fiber-optic thermometer (T4 probe and FOTEMP1-H readout, Optocon (Germany)) was suspended centrally within the upper portion of the sample under evaluation in-line with the recommendations for thermometer positioning made in [31]. By measurement of pure water samples, temperature invariance of the sample space over the first 300 s of measurement time was established.

As the water sample does not generate heat under alternating magnetic field excitation, this shows that the heat generated by the coil does not penetrate the insulation layer and enter the nanoparticle space over this time period during continuous field operation. Thus, measurements of 300 s or shorter are unaffected by heat from the excitation coil.

3.3. Magnetic particle spectrometer (MPS-3, Bruker)

The MPS-3 measures the non-linear dynamic magnetic response of the sample, and is commonly used for evaluation of potential MPI tracer materials. To do this, a sinusoidal excitation field (25 kHz, 0–25 mT) is applied, and the response is detected by a gradiometric pickup coil. Like MPI, MPS measurements contain detailed information about the nanoparticles being studied, and their local environment (including their binding state and local temperature). The gradient field found in MPI scanners for spatial encoding is not present in the MPS, this means that the MNP samples experience a rapidly changing, but approximately homogeneous field. The MPS-3 is designed to measure low-volume samples (typically around 30 μL), and incorporates a system for controlling the sample temperature between room temperature and 318 K based on a feedback-controlled temperature modulated air-flow. The sensitivity of the system to temperature-induced changes in MNP relaxation has previously been demonstrated [35].

The MPS-3 employs a separate dedicated stream of cool air to remove heat from the excitation coil. Water samples of 300 μL loaded inside of glass test tubes and measured in the MPS at 25 mT amplitude for prolonged periods show no temperature change when monitored using a fiber-optic thermometer. Thus, we are confident that heat from the excitation field generation does not leak into the sample space and influence samples.

While well optimized for highly sensitive and stable calibrated measurements of magnetic particle spectra, the MPS is a poor apparatus for the measurement of heating induced within MNP samples by the excitation field. The system was designed to minimize thermal changes within the sample. The lack of thermal insulation around the sample holder, and constant airflow around the MPS sample space, mean that heat escapes too readily from samples to be measured. The system is designed to measure very small samples, from which heat quickly dissipates.

The possibility of attempting to measure sample heating within the MPS using larger volume samples contained within glass test tubes was considered but dismissed. The method earlier described for measuring a water-filled test tube with a fiber-optic thermometer does not translate to the measurement of MFH in the system. The test tube method requires a large sample volume to be used (several hundred μL) to ensure that the thermometer probe can be reliably submerged. However, the homogeneous region of the MPS-3 excitation field is relatively small, covering a region of $2 \times 2 \times 2\,mm^3$, or 8 μL. Thus, the majority of the MNP sample destined for a test-tube based MPS hyperthermia measurement will lie outside of the homogeneous field region, and so experience lower field amplitudes than the set value. If a large part of the sample volume is experiencing an unknown reduction in the field amplitude as compared with the intended value, then measurements of field-induced MFH within the MPS will be underestimated. For these reasons, a dedicated LF-MFH system was developed for the measurement of heat generated by MNP samples.

3.4. Method

The heating efficiency of liquid and gelatin based FCT preparations was tested in the LF-MFH system at varying excitation field amplitudes. A linear fit was used to calculate the initial gradient at the onset of heating within a time span of 5 s for each LF-MFH curve. This gradient was then used as a measure of the heating efficiency in each measurement.

Temperature-dependent MPS measurements were conducted on dilute FCT-GEL samples. Solidified gelatin samples were loaded into the cool MPS-3, and the temperature of the sample space was gradually increased by the heated airflow. Samples were heated up to a maximum temperature of 318 K. The melting temperature of gelatin is dependent upon concentration and other factors, but is typically below 308 K. Upon removal of the sample from the MPS, the transition of the gelatin into a liquid state was verified by eye. The melted samples formed a slightly viscous liquid, in which the MNPs were more able to move and align with the field as compared with the solidified case. The spectra at varying temperatures were then analyzed for evidence of the melting transition occurring. Temperature-dependent MPS measurements were repeated at varying excitation field amplitudes to probe how this influenced the observed melting behavior as a result of differing particle-matrix interactions.

4. Results

4.1. Measuring LF-MFH in FCT samples

Example heating curves obtained via LF-MFH measurements of FCT preparations are shown in Fig. 2(a). When a 400 μL sample of concentrated FCT-LIQ (935 mmol/L concentration) was excited in a 10 mT field for 300 s (black curve), a bulk temperature rise of 40 K was recorded. The excitation field produced a significant bulk heating effect within the concentrated FCT sample, despite the low excitation frequency compared to therapeutic MFH. The heating curves obtained from the same sample at excitation fields of 6 mT and 3 mT are shown in red and blue in Fig. 2(a). A clear trend is observed, with larger

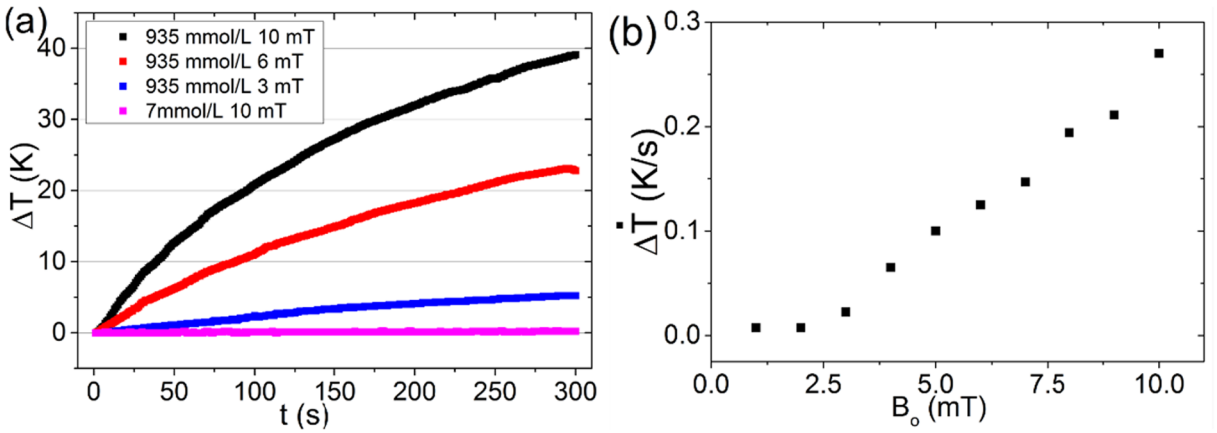

Fig. 2. (a) Example LF-MFH heating curves obtained for concentrated (black, red and blue) and dilute (pink) FCT-LIQ samples at different field amplitudes. (b) Excitation-amplitude dependence of the initial slope ($\Delta\dot{T}$) of the MF-MFH heating curves for the concentrated FCT-LIQ sample.

excitation field amplitudes producing larger heating rates and higher final temperatures. The initial heating gradient ($\Delta\dot{T}$) of concentrated FCT-LIQ at all measured amplitudes is plotted in Fig. 2b. We observe a roughly linear increase in the heating efficiency at field amplitudes between 2 mT and 10 mT.

The pink line in Fig. 2(a) shows the heating curve for a sample of dilute FCT-LIQ when measured at 10 mT excitation field. Here, no measurable heating is observed over the course of the 300 s measurement, despite the maximum excitation field amplitude. LF-MFH of a dilute FCT-GEL sample was also tested, with no measurable heating being detected. As the results for dilute FCT-LIQ and FCT-GEL are indistinguishable from each other (both $\Delta T = 0$), only the curve for dilute FCT-LIQ is plotted in Fig. 2(a).

4.2. Temperature dependent MPS at a single field amplitude

A plot of the evolution of the 3rd harmonic amplitude (A_3) and phase (φ_3) with increasing temperature is shown in Fig. 3(a) for a dilute FCT-GEL sample measured with a 25 mT excitation field. The initial A_3 and φ_3 values at 293 K were $A_3 = 170\ \mathrm{nAm^2}$ and $\varphi_3 = -16.6^{\circ}$. The percentage change in A_3 compared with the initial value (293 K) is plotted to emphasize the large scale of the observed effects. The percentage change values were calculated using

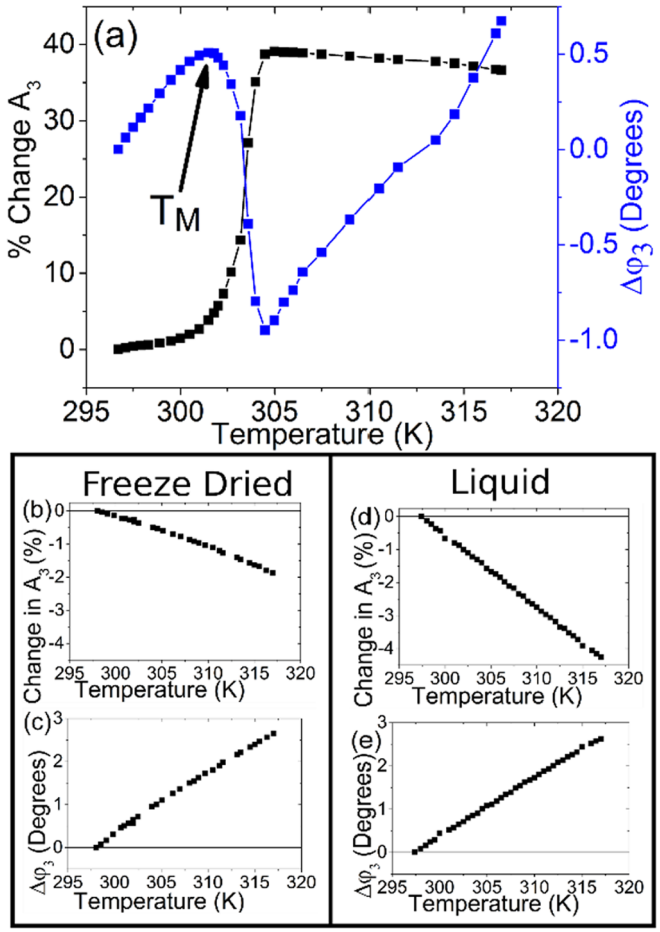

Fig. 3. Temperature dependence of MPS measurements at 25 mT. (a) FCT-GEL sample, % change in A_3 (left axis) and $\Delta\varphi_3$ (right axis) of 3rd harmonic with increasing temperature. Onset of melting transition T_M marked. (b–c)% change in A_3 and $\Delta\varphi_3$ with increasing temperature for freeze dried FCT sample. (d–e)% change in A_3 and $\Delta\varphi_3$ with increasing temperature for a low concentration liquid FCT sample.

$$\%\ Change\ \ A3 = \left(\frac{A_3(T_1) - A_3(T_0)}{A_3(T_0)}\right) \times 100$$

where $A_3(T_1) = A_3$ value at measured temperature T_1 and $A_3(T_0)$ = Initial A_3 measured at the lowest temperature T_0.

The absolute change in phase lag $\Delta\varphi_3$ with increasing temperature is presented in degrees (phase values are negative by convention, indicating the phase lag of the net magnetic moment to the excitation field). $\Delta\varphi_3$ at a given temperature is found by subtracting the φ_3 value measured at the initial temperature $\varphi_3(T_0)$ from the value measured at the new temperature $\varphi_3(T_1)$

$$\Delta\varphi 3 = \varphi 3(T_1) - \varphi 3(T_0)$$

The primary features of interest in the Fig. 3(a) are the large transitions observed simultaneously in both A_3 and φ_3. These transitions show the point at which the majority of the MNPs within the sample go from an immobilized state to a mobile one as the gelatin melts. During melting, A_3 amplitude increases by 40%, The melting transition disrupts the φ_3 significantly, where a sudden change of the phase lag occurs. In this work, we use the maximum in $\Delta\varphi_3$ at the start of the melting transition to define the melting temperature T_M (or onset of the melting event). Using this definition, for an excitation field of 25 mT amplitude, we observe $T_M = 301.7$ K.

At temperatures below the melting transition in Fig. 3(a), a gradual increase in A_3 is observed, and a steady decrease in φ_3 value. After the melting transition, the trend in the A_3 value is observed to reverse, with a small but steady decrease in the value with increasing temperature. After melting, the phase lag decreases linearly. In Fig. 3(b–e) we present the temperature dependences of A_3 and φ_3 measured via MPS at 25 mT for FCT nanoparticles in both freeze-dried (immobilized) and liquid (mobile) preparations. Comparing the results in 3(b–e) with 3(a), we observe a correlation in temperature dependence (increasing or decreasing) for the A_3 and φ_3 in the immobilized (freeze-dried and solidified FCT-GEL) and liquid (liquid and melted FCT-GEL) states. The immobilized A_3 results are the only exception to this accordance. Here, the freeze-dried A_3 shows the opposite temperature dependence (decreasing) to that observed in the solidified FCT-GEL sample (increasing).

Treated appropriately, the behavior of individual samples of dilute FCT-GEL was found to be reproducible during thermal cycling in the MPS-3. With appropriate sample handling, as described in the materials and methods section, a standard deviation in the melting transition temperature of $\sigma = 0.2$ K was achieved.

4.3. Modulation of particle-matrix interactions via the excitation field amplitude

After establishing the temperature-dependence of MPS signals obtained from dilute FCT-GEL samples using a single excitation field, the influence of varying excitation amplitudes was then investigated. Temperature-dependent MPS measurements at different excitation field amplitudes are shown in Fig. 4 for both A_3 (a) and φ_3 (b). Here, ΔA_3 is plotted, calculated in the same manner as described for $\Delta\varphi_3$. A reduction in the onset of the φ_3 melting transition T_M is observed with increasing field amplitude. A shift of approximately 2.3 K towards lower T_M temperatures results when the excitation amplitude is increased from 6 mT to 25 mT.

The excitation-amplitude dependence of the T_M melting onset is plotted in Fig. 4(c) for the available data. A significantly larger shift in the transition temperature was observed between 6 mT and 12 mT, as compared with between 12 mT and 25 mT. This suggests that the effect may saturate at higher excitation field amplitudes, although additional measurements would be required to confirm this.

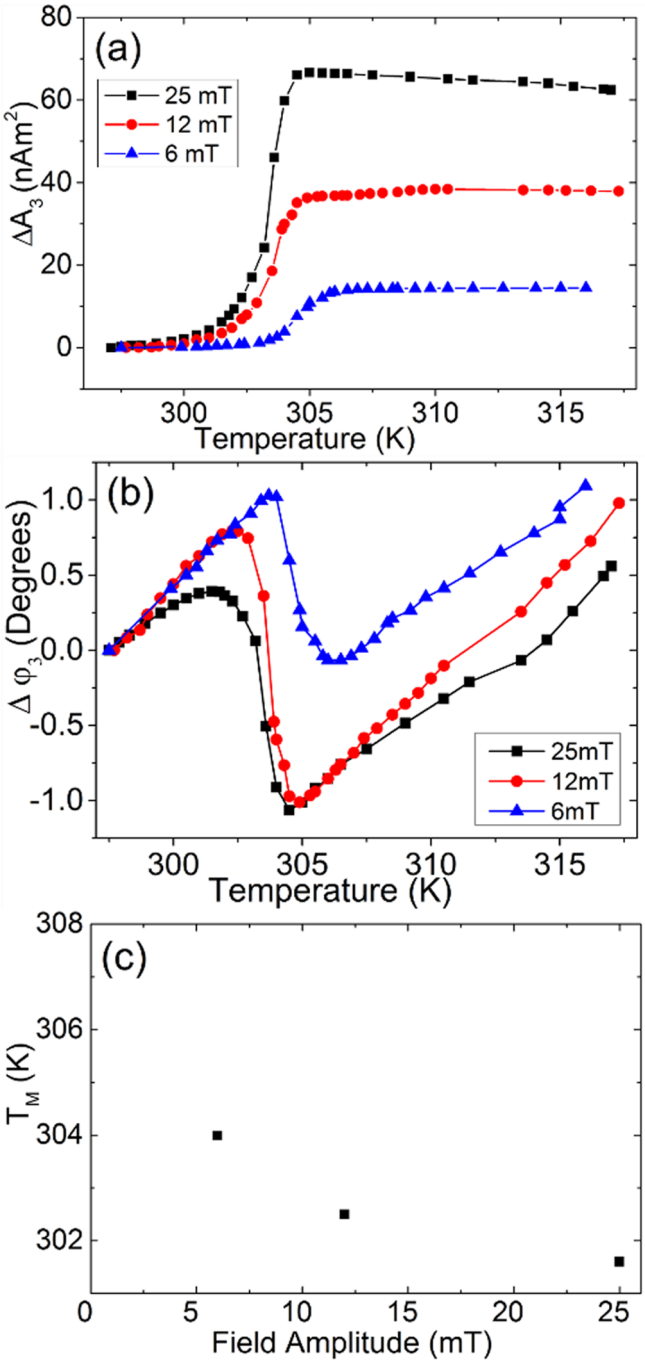

Fig. 4. Influence of the excitation field amplitude on (a) ΔA_3 and (b) $\Delta\varphi_3$ of temperature-dependent MPS measurements. (c) Extracted T_M values from measurements presented in (b).

5. Discussion

Dilute dispersions of MNPs in gelatin provide an easily-accessible and cheap platform for studying particle-matrix interactions. While other dispersion media may require less rigorous experimental controls, and provide additional stability, the melting transition of gelatin makes it well-suited for studying processes in the biologically-relevant temperature range.

The LF-MFH measurements (Fig. 2(a)) demonstrated that while significant heating may be recorded at a given frequency and amplitude for a concentrated FCT sample, a reduction in the FCT concentration can result in no measurable heating from the same excitation field. In the case of the FCT-GEL and dilute FCT-LIQ samples measured at maximum field amplitude, heat generated by the nanoparticles dissipates into the environment without raising the macroscopic temperature of the MNP suspension (as illustrated in Fig. 1(e)). The nonlinear behavior observed at low excitation field amplitudes in Fig. 2(b) may be caused either by heat dissipating too quickly from the sample to be detected, or it may be the case that the particles do not produce even local heating at such small amplitudes.

For FCT-GEL, an excitation field of 25 mT resulted in $T_M = 301.7$ K, while a 6 mT excitation gave $T_M = 304$ K. These values are lower than the literature value for gelatin melting (< 308 K [36]). The lower values recorded in this study may be partly explained by the addition of MNPs changing the melting temperature, and also by localized effects caused by the excitation field. In [9], a melting transition onset of ~305 K was recorded for iron oxide MNPs of unspecified iron concentration dispersed in 4 % gelatin. T_M values are likely to be highly sensitive to the gelatin source and preparation procedure, as well as the type and concentration of MNPs added. In this study, all Gelatin samples were taken from the same batch of FCT-GEL, thus the properties of the FCT-GEL material should be homogeneous for all measurements.

The shift towards lower T_M values at higher excitation fields suggests that energy dissipated by the nanoparticles is influencing the melting behavior of the FCT-GEL samples. Since no macroscopic heating is observed in the LF-MFH measurements of FCT-GEL samples, the observed shift in T_M with excitation amplitude is evidence for local heating or mechanical strain effects in the immediate vicinity of MNPs. Additional measurements should be undertaken to further explore the observed dependences, and investigate their origins.

The increase in A_3 amplitudes during the FCT-GEL melting transition are a result of the number of particles which are free to rotate, and thus contribute to the overall signal increasing. The increase in the phase lag during melting might be at first counterintuitive, as the additional availability of the Brownian processes after melting might be expected to facilitate a reduced phase lag. One possibility for the observed φ_3 behavior during melting could be disruption resulting from interactions between particles. For example, freed MNPs could form dipolar chains which would inhibit the magnetization rotation. Additional measurements (e.g. frequency dependence and different particle systems) would be needed to investigate the true cause.

The solidified FCT-GEL and freeze-died samples might be expected to exhibit similar temperature dependences, as nanoparticles in each are immobilized by the surrounding matrix. The observation of opposite trends in the A_3 of each sample (Fig. 3(a-b)) may be explained by the immobilization offered by gelatin being less complete than that offered by the freeze-drying process. Especially at higher field amplitudes, some MNPs may be able to gradually rotate within the gelatin matrix to align with the field, and increase the signal amplitude. In addition, the distribution of different particle sizes, magnetic moments, magnetic core arrangements and other characteristics mean that different MNPs in the sample will interact differently with the surrounding matrix. As a result, some nanoparticles may break free from their local matrix (via mechanical strain, heating, or a combination thereof) before others. This may explain the gradual creep upwards in the solidified FCT-Gel A_3 before the main melting transition. Additional measurements would be required to test this hypothesis.

The authors stress that the reported evidence for nanoscale effects during MPS of FCT-GEL samples does not necessarily mean that MPS or MPI measurements impact in any negative way on living tissue. However, the measurable shifts in melting behavior at different excitation fields suggest that additional studies should be undertaken to test the impact of MPS and MPI measurements on their local environment during MPI and MPS. These studies should test for cell reactions including oxidative stress, cytokine response, the tracking of heat-shock proteins, and physical damage to cell membranes. The minimization of cell stress as a result of local particle-matrix interactions induced by MPI or MPS excitation fields may become a key consideration in the

future design and development of MPI tracers and scanners.

It should be noted that the disparity between the frequencies in the MPS-3 and LF-MFH measurements reported here is not ideal. To improve the study, heating and MPS measurements conducted at the same frequency, (or even in the same measurement system) would be optimal. Work is currently underway to expand the frequency range available in the LF-MFH apparatus to allow measurements across a wide range of frequencies (including 25 kHz to match the MPS-3). The authors anticipate the publication of further studies including LF-MFH results at 25 kHz and other frequencies at a later date.

The measurements reported here have only dealt with single-axis, single-frequency homogeneous excitation fields provided by the MPS-3. The frequency dependence of the MPS FCT-GEL melting measurements should also be studied in future work. Suitable MPS systems with variable frequencies are already operational within other research groups [36]. Further studies should also be conducted to investigate the particle-matrix interaction in the presence of the typical 3-axis excitation fields and additional strong magnetic field gradients of up to 2.5 T/m commonly used in commercially available preclinical MPI scanners. Measurements should also be expanded to study the particle-matrix interactions of other MNP tracers during MPS and MPI.

6. Conclusion

Experimental evidence has been presented for the detectable modulation of particle-matrix interactions via the amplitude of the MPS excitation field. For FCT particles, LF-MFH measurements of high concentration samples demonstrated that individual MNPs do dissipate sufficient heat into their surroundings to produce a bulk macroscopic temperature rise. Measurements of low concentration samples using the same excitation fields showed that no macroscopic heating was produced, despite the particles still undergoing the same dissipative relaxation process. Temperature dependent MPS measurements were used to probe the melting behavior of dilute FCT-GEL samples, with a clear signature of the melting event present in both the A_3 and φ_3. The onset of the FCT-GEL melting transition was found to occur at lower MPS temperatures for larger excitation field amplitudes. Between excitation amplitudes of 6 mT and 25 mT, a 2.3 K shift in the onset of the melting transition was observed. At present, our measurements do not extend to lower excitation amplitudes, but we extrapolate that the real shift in melting behavior between zero-field and 25 mT will be even larger. So far, our measurements are unable to differentiate between effects arising from local microscopic heating close to individual nanoparticles, mechanical forces exerted on the immobilizing matrix, or other unknown contributions. Nevertheless, our results suggest that careful evaluation of the microscopic cellular impact of MPI and MPS measurements should be undertaken, to verify whether the particle-matrix interactions translate into real physiological strain.

Acknowledgements

The financial support of the DFG research grants “quantMPI: Establishment of quantitative Magnetic Particle Imaging (MPI) application oriented phantoms for preclinical investigations“ (TR 408/9-1) and “AMPI: “Magnetic particle imaging: Development and evaluation of novel methodology for the assessment of the aorta in vivo in a small animal model of aortic aneurysms” (SHA 1505-2/1) as well as the DFG priority program “SPP 1681: Metrology for biomedical applications of magnetic hybrid materials” (WI 4230/1-3) are gratefully acknowledged. This work was additionally funded by the EMPIR program co-financed by the Participating States and from the European Union’s Horizon 2020 research and innovation program “MagNaStand: Towards an ISO standard for magnetic nanoparticles” (grant no. 16NRM04), and the Federal Ministry of Economics and Technology within the TransMeT project “Magnetische Messtechnik für die Größenfraktionierung magnetischer Nanopartikel”.

References

[1] B. Gleich, J. Weizenecker, Tomographic imaging using the nonlinear response of magnetic particles, Nature 435 (7046) (2005) 1214–1217.
[2] T. Knopp, N. Gdaniec, M. Möddel, Magnetic particle imaging: from proof of principle to preclinical applications, Phys. Med. Biol. 62 (2017).
[3] N. Panagiotopoulos, et al., Magnetic particle imaging: current developments and future directions, Int. J. Nanomed. 10 (2015) 3097–3114.
[4] M. Graeser, et al., Towards picogram detection of superparamagnetic iron-oxide particles using a gradiometric receive coil, Sci. Rep. 7 (2017) 6872.
[5] H. Paysen, et al., Improved sensitivity and limit-of-detection using a receive-only coil in magnetic particle imaging, Phys. Med. Biol. 63 (13) (2018).
[6] J. Haegele, et al., Multi-color magnetic particle imaging for cardiovascular interventions, Phys. Med. Biol. 21 (16) (2016) 415–426.
[7] C. Stehning, Bernhard Gleich, J. Rahmer, Simultaneous magnetic particle imaging (MPI) and temperature mapping using multi-color MPI, Int. J. Magn. Part. Imag. 2 (6) (2016).
[8] Y. Muslu, M. Utkur, O.B. Demirel, E.U. Saritas, Calibration-Free relaxation-based multi-color magnetic particle imaging, IEEE Trans. Med. Imag. 37 (8) (2018) 1920–1931.
[9] E.I. Wisotzki, D. Eberbeck, H. Kratz, S.G. Mayr, Magnetic response of gelatin ferrogels across the sol-gel transition: the influence of high energy crosslinking on thermal stability, Soft Matter 12 (2016) 3908–3918.
[10] A. Tschöpe, K. Birster, B. Trapp, P. Bender, R. Birringer, Nanoscale rheometry of viscoelastic soft matter by oscillating field magneto-optical transmission using ferromagnetic nanorod colloidal probes, J. Appl. Phys. 116 (18) (2014) pp.
[11] A. Lindemann, K. Lüdtke-Buzug, B.M. Fräderich, K. Gräfe, R. Pries, B. Wollenberg, Biological impact of superparamagnetic iron oxide nanoparticles for magnetic particle imaging of head and neck cancer cells, Int. J. Nanomed. 29 (9) (2014) 5025–5040.
[12] P. Vogel, M.A. Rï¿½ckert, P. Klauer, W.H. Kullmann, P.M. Jakob, V.C. Behr, First in vivo traveling wave magnetic particle imaging of a beating mouse heart, Phys. Med. Biol. 61 (18) (2016) 6620–6634.
[13] J. Weizenecker, B. Gleich, J. Rahmer, H. Dahnke, J. Borgert, Three-dimensional real-time in vivo magnetic particle imaging, Phys. Med. Biol. 54 (5) (2009) L1–L10.
[14] B. Zheng, et al., Magnetic particle imaging tracks the long-term fate of in vivo neural cell implants with high image contrast, Sci. Rep. 5 (2015) 14055.
[15] B. Zheng, et al., Quantitative magnetic particle imaging monitors the transplantation, biodistribution, and clearance of stem cells in vivo, Theranostics 6 (3) (2016) 291–301.
[16] J. Rahmer, et al., Nanoparticle encapsulation in red blood cells enables blood-pool magnetic particle imaging hours after injection, Phys. Med. Biol. 58 (12) (2013).
[17] W.C. Poller, et al., Magnetic particle spectroscopy reveals dynamic changes in the magnetic behavior of very small superparamagnetic iron oxide nanoparticles during cellular uptake and enables determination of cell-labeling efficacy, J. Biomed. Nanotechnol. 12 (2) (2016) 337–346.
[18] N. Löwa, P. Knappe, F. Wiekhorst, D. Eberbeck, A.F. Thunemann, L. Trahms, How hydrodynamic fractionation influences MPI performance of resovist, IEEE Trans. Magn. 51 (2) (2015).
[19] C. Blanco-Andujar, D. Ortega, P. Southern, Q.A. Pankhurst, N.T.K. Thanh, High performance multi-core iron oxide nanoparticles for magnetic hyperthermia: microwave synthesis, and the role of core-to-core interactions, Nanoscale 7 (5) (2015) 1768–1775.
[20] P. Hugounenq, et al., Iron oxide monocrystalline nanoflowers for highly efficient magnetic hyperthermia, J. Phys. Chem. C 116 (29) (2012) 15702–15712.
[21] M. Bañobre-López, A. Teijeiro, J. Rivas, Magnetic nanoparticle-based hyperthermia for cancer treatment, Rep. Pract. Oncol. Radiother. 18 (6) (2013) 397–400.
[22] K. Maier-Hauff, et al., Efficacy and safety of intratumoral thermotherapy using magnetic iron-oxide nanoparticles combined with external beam radiotherapy on patients with recurrent glioblastoma multiforme, J. Neurooncol. 103 (2) (2011) 317–324.
[23] M. Johannsen, et al., Clinical hyperthermia of prostate cancer using magnetic nanoparticles: presentation of a new interstitial technique, Int. J. Hyperth. 21 (2005) 637–647.
[24] A. Chiu-Lam, C. Rinaldi, Nanoscale thermal phenomena in the vicinity of magnetic nanoparticles in alternating magnetic fields, Adv. Funct. Mater. 26 (22) (2016) 3933–3941.
[25] G.F. Goya, L. Asín, M.R. Ibarra, Cell death induced by ac magnetic fields and magnetic nanoparticles: current state and perspectives, Int. J. Hyperth. 29 (8) (2013).
[26] R. Mansell, et al., Magnetic particles with perpendicular anisotropy for mechanical cancer cell destruction, Sci. Rep. 7 (1) (2017) 4257.
[27] D.W. Wong, W.L. Gan, Y.K. Teo, W.S. Lew, Interplay of cell death signaling pathways mediated by alternating magnetic field gradient, Cell Death Discov. 4 (49) (2018).
[28] C. Kuhlmann, et al., Drive-field frequency dependent MPI performance of single-core magnetite nanoparticle tracers, IEEE Trans. Magn. 51 (2) (2015) 6500504.
[29] A. Lak, T. Wawrzik, F. Ludwig, M. Schilling, Synthesis of single-core iron oxide nanoparticles as a tracer for magnetic particle imaging, Springer Proceedings in Physics, (2012).
[30] S.S. Shevkoplyas, A.C. Siegel, R.M. Westervelt, M.G. Prentiss, G.M. Whitesides, The force acting on a superparamagnetic bead due to an applied magnetic field, Lab Chip 7 (10) (2007) 1294–1302.
[31] R.R. Wildeboer, P. Southern, Q.A. Pankhurst, On the reliable measurement of specific absorption rates and intrinsic loss parameters in magnetic hyperthermia

materials, J. Phys. D Appl. Phys. D 47 (49) (2014) pp.
[32] Y.-X.J. Wang, Superparamagnetic iron oxide based MRI contrast agents: current status of clinical application, Quant. Imag. Med. Surg. 1 (1) (2011) 35–40.
[33] J. Wells, et al., Standardisation of magnetic nanoparticles in liquid suspension, J. Phys. D. Appl. Phys. 50 (38) (2017).
[34] E. Natividad, M. Castro, A. Mediano, Adiabatic vs. non-adiabatic determination of specific absorption rate of ferrofluids, J. Magn. Magn. Mater. 321 (10) (2009) 1497–1500.
[35] J. Wells, H. Paysen, O. Kosch, L. Trahms, F. Wiekhorst, Temperature dependence in magnetic particle imaging, AIP Adv. 8 (5) (2018).
[36] Z.W. Tay, P.W. Goodwill, D.W. Hensley, L.A. Taylor, B. Zheng, S.M. Conolly, A high-throughput, arbitrary-waveform, MPI spectrometer and relaxometer for comprehensive magnetic particle optimization and characterization, Sci. Rep. 6 (34180) (2016).